Ilam University of Medical Sciences

Journal of Basic Research in Medical Sciences

Online ISSN: 2383-0972
Print ISSN: 2383-0506

Homepage: https://jbrms.medilam.ac.ir

Calculation of photoneutron contamination of Varian linac with new target in tissue equivalent phantom using Monte Carlo simulation

Mojtaba Cheraghian[1], Tayyeb Pourfallah[2,3]✉, Amir Abbas Sabouri-Dodaran[1], Mehrdad Gholami[4]

[1]Department of Physics, Payame Noor University, P.O. Box 19395-4697, Tehran, Iran
[2]Department of Biochemistry, Biophysics and Genetics, Medical College, Mazandaran University of Medical Sciences, Sari 48157-33971, Iran
[3]Department of Medical Physics, Mazandaran University of Medical Sciences, 48157-33971, Sari, Iran
[4]Department of Medical Physics, School of Allied Medical Sciences, Lorestan University of Medical Sciences, Khorramabad 68138-33946, Iran

Article Info

Article type:
Research Article

Article history:
Received: 30 Mar. 2022
Revised: 30 Apr. 2022
Accepted: 18 May. 2022
Published online: 14 Nov. 2022

✉**Correspondence to:**
Dr. Tayyeb Pourfallah, Department of Medical Physics, Medical College, Pyambar Azam Academic Complex, Mazandaran University of Medical Sciences (MAZUMS), P.O Box 48157-33971, Sari, Iran
Tel: +98 11 33543256
Fax: +98 11 33352725
Email: tpourfallah@mazums.ac.ir

ABSTRACT

Introduction: In this research, a new material ($Ti_2V_{0.7}Cu_{97.3}$) was proposed for the target of medical linear accelerators (linacs) to reduce the production of unwanted photoneutrons in the radiotherapy. So, the fluence, dose equivalent and kerma of the photoneutrons were calculated in a soft tissue phantom.

Materials and Methods: The medical linac was the Varian 2100 C/D 18 MV, which its tungsten target was replaced with a new multi-metal target ($Ti_2V_{0.7}Cu_{97.3}$). Desired quantities were computed in a ICRU soft tissue phantom, using the Monte Carlo code MCNPX (v. 2.6).

Results: The ratio of the maximums of fluence, kerma, and dose equivalent of photoneutrons along the central axis of the ICRU phantom with new target rather than tungsten target were 72 %, 59 % and 61 %, respectively. Average of the Ratio of fluence, kerma, and dose equivalent in inner area (distances less than 5 cm from central axis) at different depths of the phantom with new target rather than tungsten target were 78 %, 70 % and 75 %, respectively. Uncertainties at all points were less than 5 % (except for a few points which were less than 10 %).

Conclusion: This work showed that applying $Ti_2V_{0.7}Cu_{97.3}$ alloy for the target of linac, can reduce the produced photoneutrons up to 38 % by an applicable and inexpensive way.

Keywords: MCNPX, Photoneutron contamination, Simulation, Target of linac

How to cite this article: Cheraghian M, Pourfallah T, Sabouri-Dodaran AB, Gholami M. Calculation of photoneutron contamination of Varian linac with new target in tissue equivalent phantom using Monte Carlo simulation. J Bas Res Med Sci. 2022; 9(3):31-41.

Publisher: Ilam University of Medical Sciences

Introduction

Medical linear accelerators (linacs) are used for treating compact tumors extensively. Head of linacs mainly constructed of heavy elements such as lead, tungsten, iron, cupper and so on. When the applied energy is more than the threshold energy of (γ, n) or (e, n) reactions, (~ 8

MeV), some undesired photoneutrons and electroneutrons are produced which can deliver additional dose to patients, which possibly can cause secondary cancers after radiotherapy. Since quality factor of neutrons is about 2 - 20 times more than photons (i.e., varies with neutron energy) (1), they have a substantially higher biological effectiveness than photons. Therefore, even a small number of neutrons can lead to a non-negligible effective dose to patients, in the form of non-target and out-of-field dose (2).

Interactions between high energy treatment beam and nuclei of composing elements of the linac, beam collimation system, couch, patient's body, air and walls of treatment room can produce photoneutrons. Because the threshold energy of (γ, n) reaction for composing elements of the head of linac, such as lead, tungsten, copper and iron, is generally in the range of 6.74 - 11.20 MeV, interactions between high energy treatment beam and nuclei of composing elements of the medical linear accelerator (linac), couch, patient's body, air and walls of treatment room can produce photoneutrons (3).

Estimation of photoneutron contamination in radiotherapy (RT) has been studied by several researchers in various experimental and simulation methods (4-10). Bezak and his coworkers (11, 12) measured the total dose equivalent in Rando and water equivalent phantoms, using TLD and estimated the risk of secondary cancer in organs of Rando phantom in treatment of prostate. Sohrabi and Hakimi measured the dose of thermal and epithermal photoneutrons using a self-made experimental method within a polyethylene phantom (13). Bagheri et al. (14) and Bagheri et al. (15) measured the dose of thermal photoneutrons in treatment of breast cancer within the breast Rando phantom using TLD. Comparing the experimental results for photoneutron contamination show differences between results. It has been demonstrated that using the Monte Carlo code MCNPX, in radiotherapy, can lead to reliable outputs and are accordance with experimental measurements. Barquero et al., (16) calculated the effects of total photoneutrons on various organs using MCNPX code in a computational phantom. Many others calculated the spectra of photoneutrons and dose equivalent(DE) due to photoneutrons in tissue (17-21). and some of them (18, 22) calculated the DE of fast neutrons in voxel-based phantoms. Calculating the effects of each category of photoneutrons along the beam axis, in water equivalent and water phantoms were conducted by many other researchers (4, 5, 23-28).

According to published researches, different materials and thickness of target have influence on dose rate and production of photoneutrons (29-32). Geo et al. (29) studied the effects of thickness of several materials on dose rate and leakage of electron for 6MeV electron beam.

Berger and Seltzer (30) described calculations of bremsstrahlung production and associated photoneutron production in thick targets irradiated by electron beams with energies between 10 and 60 MeV. They showed that the target plays an important role in the production of photon and yield of photoneutron.

It is shown that the main components which produce contaminant photoneutrons are primary collimator, secondary collimator and target (33, 34). Manipulation of target for reducing the photoneutron yield of a linac is more applicable and easer rather than collimators. Commonly the target of linacs is made of tungsten. In a study, Rojas-Arias et al. (31) proposed a new self-made alloy ($Ti_2V_{0.7}Cu_{97.3}$) as the target of linac. They showed when a plate of this alloy was irradiated with a 16 MeV beam of electrons, smaller number of photoneutrons produce in comparison with tungsten plate. In this research we intend to calculate the proportion of photoneutron fluence, kerma and dose equivalent of photoneutrons in axial and transverse directions within an ICRU phantom using MCNPX simulation code for the proposed target [by Rojas-

Arias et al. (31)] in 18 MV Varian linac 2100 C/D machine (hereafter new machine) and compare them with conventional machine with tungsten target (hereafter current machine). To consider the role of nitrogen and similarity to the tissue of the body, we used ICRU soft tissue equivalent phantom in simulations. Most of the researchers have studied photoneutrons distributions in the air of the treatment room and only few works studied photoneutrons within soft tissue equivalent phantom.

Materials and Methods

A typical treatment room (28) with walls, ceiling (thickness of 1.7 m) and floor (thickness of 1 m) from concrete simulated. For calculating the required quantities, the MCNPX Monte Carlo code, Version 2.6, was applied. Current and new machines are the same except the material of the target. The head of the linac including all effective components therein containing target (tungsten for current machine and $Ti_2V_{0.07}Cu_{97.93}$ for new machine), primary collimator (W), vacuum window (Be), flattening filter (Fe and Ta), ionization chamber (Cu and Kapton), secondary collimator (W and Pb), mirror (Mylar), Jaws (W), and upper circle (Fe) were simulated. The energy of linacs was 18 MeV in photon mode. The fluence, dose equivalent and kerma of photoneutrons calculated at 105 points, at axial and transvers directions of incident photon beam, within an ICRU soft tissue phantom. Field size of the treatment photon beam was 10×10 cm^2 and SSD= 100 cm. More details are in previous work (10).

F4 tally is for calculating transmitted flux of the particle in terms of number of particles per square centimeter (n.cm^{-2}), which could be converted to DE using Flux-to-Dose Rate Conversion factor and Quality Factor in terms of mSv/Gy-X (Appendix H of MCNPX user's manual). The values of these factors are related to energy of photons, and have specific amount for every range of energy. Energy ranges and conversion factors were entered to input file using "dose energy" and "dose function" cards, respectively. In this research, for this purpose, NCRP NO. 38 recommended factors were used. Kerma acquired by means of F6 tally in terms of MeV.g^{-1}/electron, which was changed to mGy.Gy^{-1}.

Results

At first, neutron source strength was calculated for new machine based on McGinley and Landry method (9). The result was 0.85×10^{12} n/Gy in comparison with 1.37×10^{12} n/Gy for current machine. These outputs obviously showed that production of photoneutrons has decreased for new machine.

The fluence, kerma, and dose equivalent of photoneutrons along the central axis at 34 points of ICRU phantom from the depth of 0.1 cm to 29 cm for current and new machine are depicted in Figure 1.

The fluence, kerma, and dose equivalent of total photoneutrons along the transvers direction at 80 points at depths of 0.1, 1, 10 and 20 cm of the ICRU phantom were shown in Figures 2-4.

Discussion

Since the elements in new alloy have lower atomic number than tungsten, it is expected that production of photoneutrons be less than tungsten, too. Calculations demonstrated this fact; the neutron source strength for new machine is 68 % of common machine.

Figure 1a shows that the amounts of fluence, kerma and dose equivalent at all points are less for new machine. These quantities decrease rapidly to depth of 15 cm (i.e., for fluence after depth of 2 cm) and then the curves become nearly constant, which is in accordance with Kry's findings (19), for tungsten target.

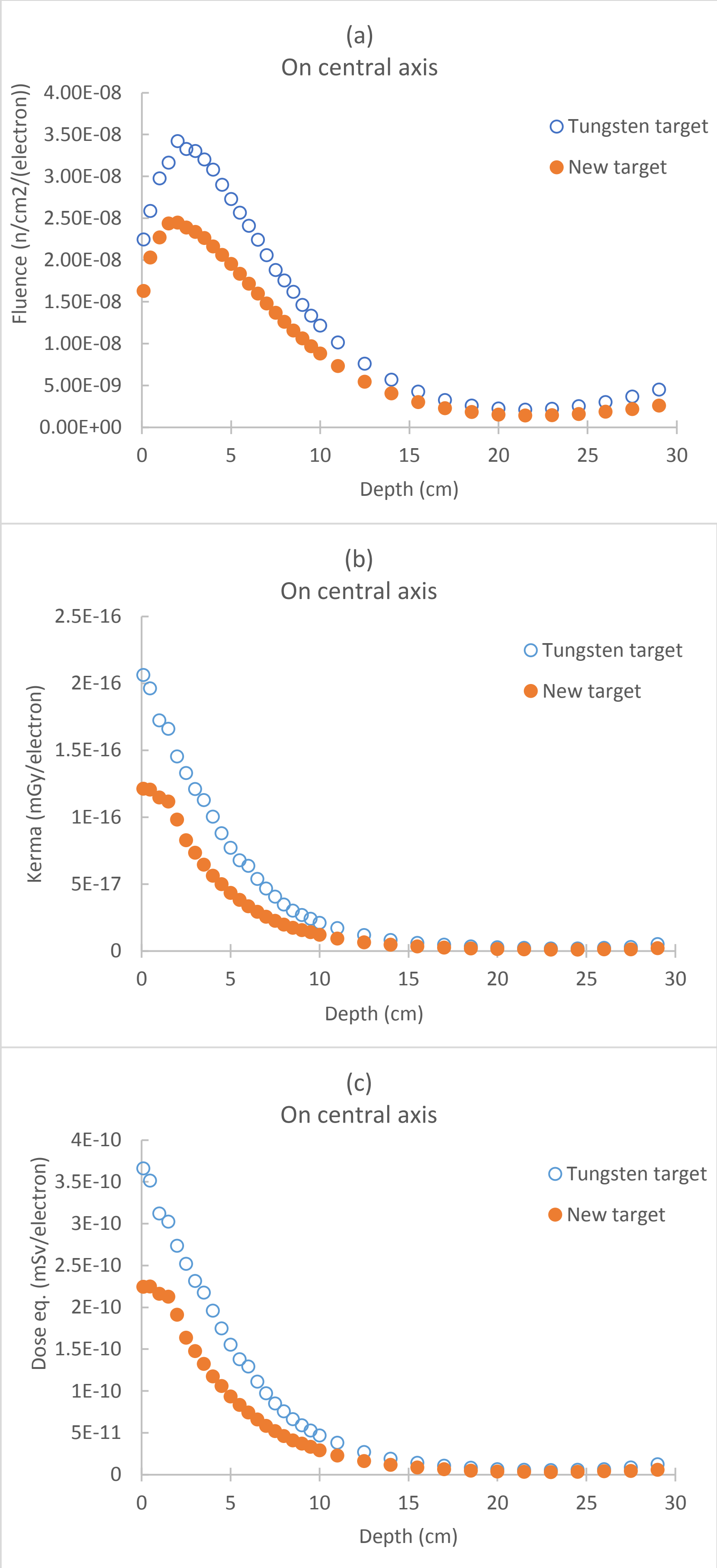

Figure 1. The (a) fluence, (b) kerma, and (c) dose equivalent of photoneutrons along the central axis of ICRU phantom for current and new machine.

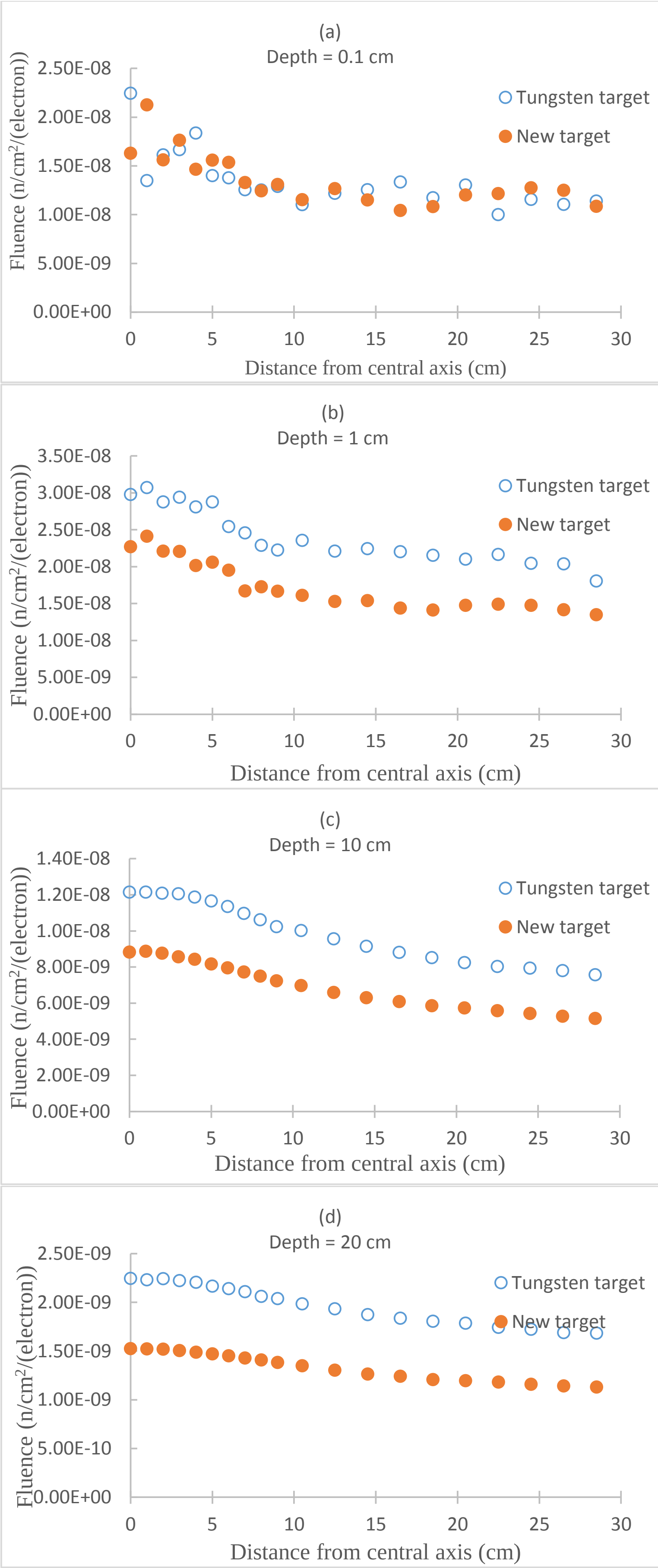

Figure 2. Fluence of photoneutrons at lateral direction in depths (a) 0.1 cm, (b) 1 cm, (c) 10 cm and (d) 20 cm.

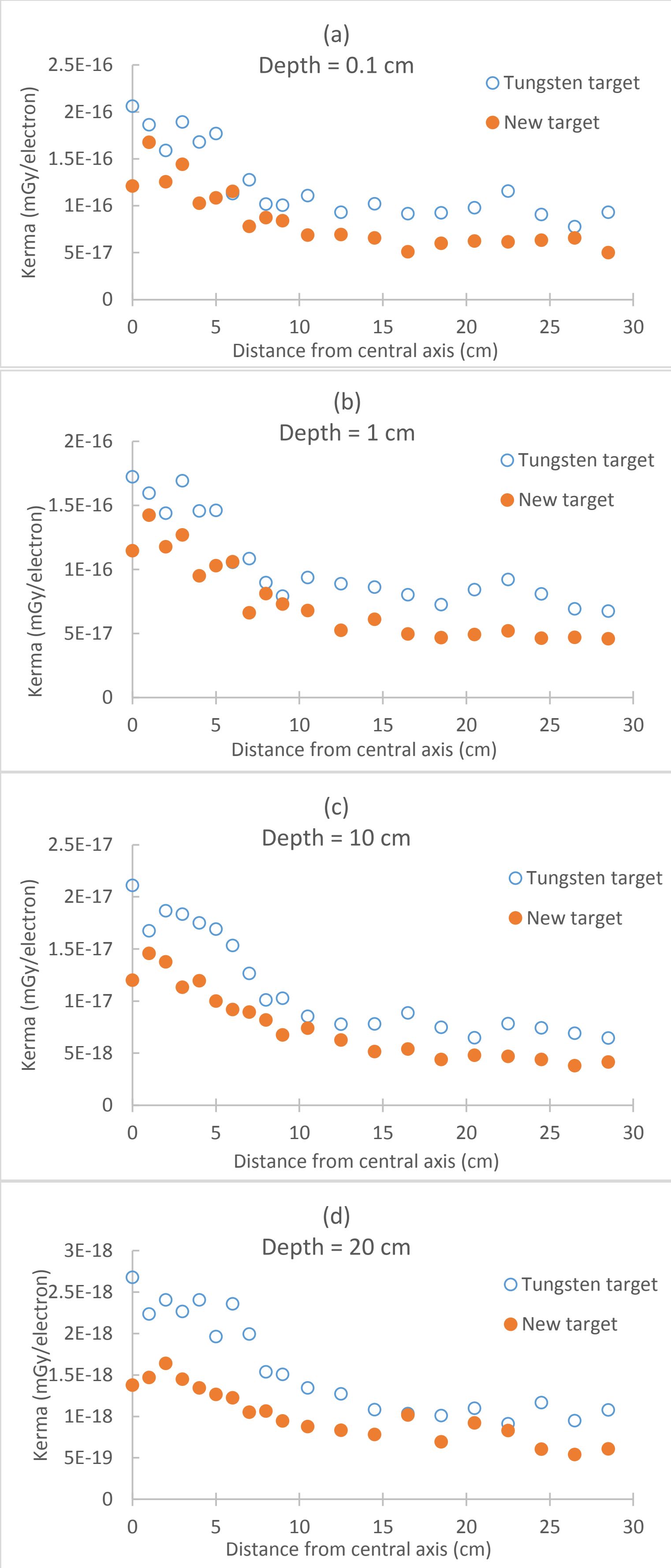

Figure 3. Kerma of photoneutrons at lateral direction in depths (a) 0.1 cm, (b) 1 cm, (c) 10 cm and (d) 20 cm.

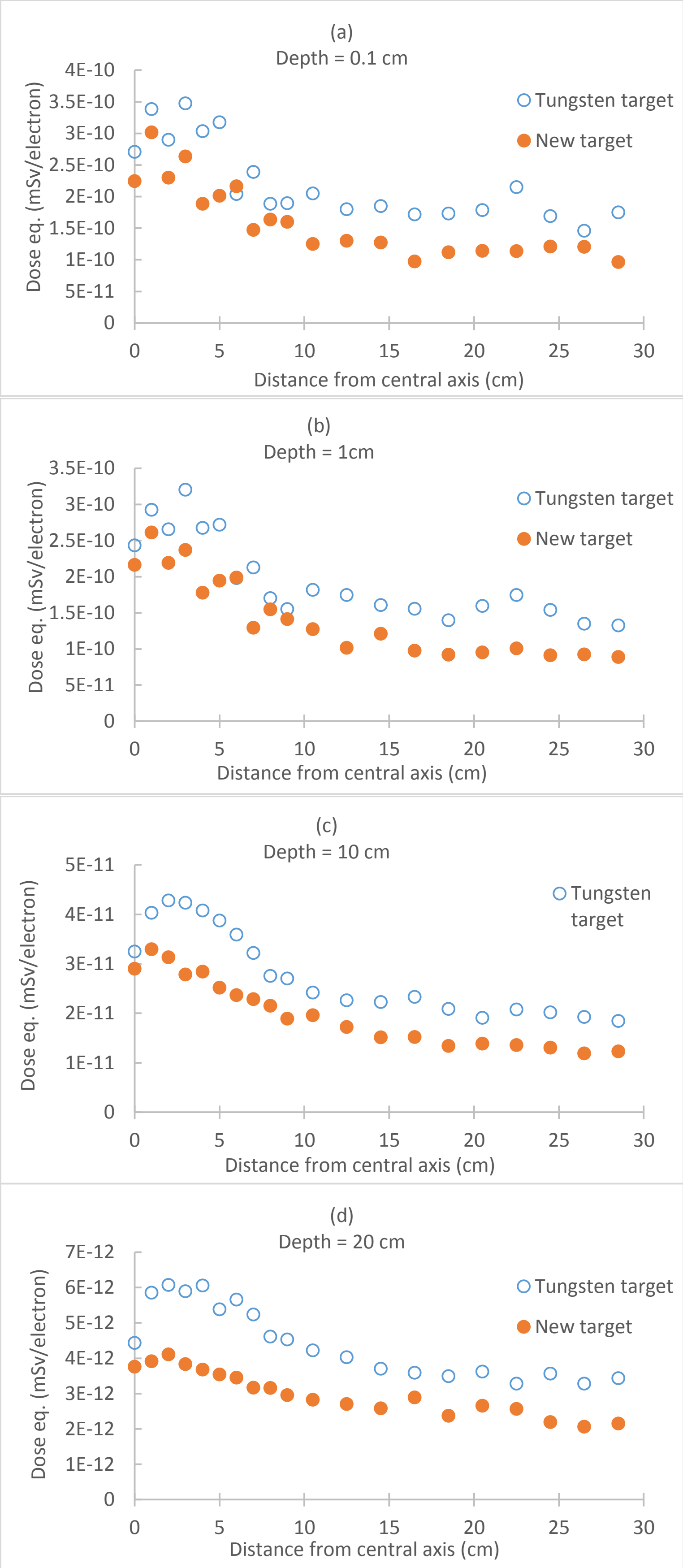

Figure 4. Dose equivalent of photoneutrons at lateral direction in depths (a) 0.1 cm, (b) 1 cm, (c) 10 cm and (d) 20 cm.

For comparing the results quantitively, the phantom was divided into two areas: depths less than 15 cm (*shallow area)* and depths more than 15 cm (*deep area)*.
Ratios of maximums of fluence, kerma, and dose equivalent at axial direction in machine with new target to machine with tungsten target are 0.72, 0.59, and 0.61, respectively. Ratio of these quantities in average at shallow and deep areas are 0.72, 0.60, 0.56; and 0.65, 0.50, 0.64, respectively. All over, these findings show all three quantities at axial directions are less in machine with new target.
Figure 2 shows the fluence of photoneutrons at lateral direction at 0.1, 1, 10 and 20 cm depths. These diagrams show that at distances less than 5 cm and distances more than 10 cm the curves are almost horizontal and at distances between 5 and 10 cm they are descending. Because the field size was 10 × 10 cm^2, so the edge of incident photon beam is at 5 cm from central axis and the number of photoneutrons is more in the photon field. So, we can divide the phantom laterally into three areas: *inner area* (distances less than 5 cm from central axis), *penumbra area* (distances between 5 and 10cm) and *outer area* (distances more than 10 cm). This manner is on expectance, because it was shown that fluence of photoneutrons is higher within the photon field (35,18).
Figures 3 and 4 shows the kerma and dose equivalent of photoneutrons at lateral direction in depths 0.1, 1, 10 and 20 cm, respectively. Kry and et al., (19) using MCNPX code have derived a curve for dose equivalent only for surface of the phantom, in the same conditions for tungsten target, and our result (dose equivalent at depth 0.1 cm) is very close to these amounts which in another paper (10) depicted and compared these two diagrams.
Ratios of fluence in average at lateral directions (i.e., at 0.1, 1, 10 and 20 cm depths) in machine with new target to machine with tungsten target at inner area (i.e., axial distances less than 5 cm) and outer area (i.e., axial distances more than 5 cm) are 0.78, and 0.74, respectively. Ratios of kerma and dose equivalent in average for new target and tungsten target at inner area and outer area are 0.70, 0.65; and 0.75, 0.66, respectively. Overall, these findings show that the fluence, kerma and dose equivalent in lateral directions are less in machine with new target.

Conclusion

Along central axis of the treatment beam, in the ICRU soft tissue phantom, the fluence, kerma, and dose equivalent of produced unwanted photoneutrons for the linac which its target is made of new alloy ($Ti_2V_{0.7}Cu_{97.3}$) are less than the linac with tungsten target.
Calculation of photoneutron production in both central axis and transverse directions within the ICRU phantom showed that photoneutron fluence, kerma and dose equivalent decreased remarkably by applying the new target in the linac and verify that this introduced alloy is suitable for setting in the head of linacs. Though this alloy mainly composed of cupper, but heat removal of cupper (401 W/m.℃) is larger in comparison with tungsten (174 W/m.℃) (31).
In future works one can calculate the photon yield as well as electron contamination of this new target, to gain more knowledge of this new machine. Authors suggest another research by applying some neutron absorbers as protective aprons during treatment and calculating or measuring the photoneutron contamination in presence of these protective materials.

Acknowledgements

Payame Noor University covered the financial costs of the present study.

Conflict of Interest

There is no conflict of interest regarding this research.

References

1. Siebert B, Schuhmacher H. Quality factors, ambient and personal dose equivalent for neutrons, based on the new ICRU stopping power data for protons and alpha particles. Radiat Prot Dosim. 1995; 58(3): 177-183. doi: 10.1093/oxfordjournals.rpd.a082612.
2. Israngkul-Na-Ayuthaya I, Suriyapee S, Pengvanich P. Evaluation of equivalent dose from neutrons and activation products from a 15-MV X-ray LINAC. J Radiat Res. 2015; 56(6): 919-926. doi: 10.1093/jrr/rrv045.
3. Alfuraih A, Chin M, Spyrou N. Measurements of the photonuclear neutron yield of 15 MV medical linear accelerator. J Radioanal Nucl Chem. 2008; 278(3): 681-684. doi: 10.1007/s10967-008-1504-y.
4. Karimi A H, Vega-Carrillo H R. Grid therapy vs. conventional radiotherapy - 18 MV treatments: Photoneutron contamination along the maze of a linac bunker. Appl Radiat Isot. 2020; 158: 109064. doi: 10.1016/j.apradiso.2020.109064.
5. Hosseinzadeh E, Banaee N, Nedaie H A. Monte Carlo calculation of photo-neutron dose produced by circular cones at 18MV photon beams. Rep Pract Oncol Radiother. 2018; 23(1): 39-46. doi: 10.1016/j.rpor.2017.12.001.
6. Ghasemi A, Pourfallah TA, Akbari M, Babapour H, Shahidi M. Photo neutron dose equivalent rate in 15 MV X-ray beam from a Siemens Primus Linac. J Med Phys. 2015; 40(2): 90-94. doi: 10.4103/0971-6203.158681.
7. Waller EJ, Jamieson TJ, Cole D, Cousins T, Jammal RB. Experimental and computational determination of neutron dose equivalent around radiotherapy accelerators. Radiat Prot Dosim. 2003; 107(4): 225-232. doi: 10.1093/oxfordjournals.rpd.a006394.
8. Lin JP, Chu TC, Lin SY, Liu MT. The measurement of photoneutrons in the vicinity of a Siemens Primus linear accelerator. Appl Radiat Isot. 2001; 55(3): 315-321. doi: 10.1016/S0969-8043(01)00084-7.
9. McGinley PH, Landry J. Neutron contamination of x-ray beams produced by the Varian Clinac 1800. Phys Med Biol. 1989; 34(6): 777. doi: 10.1088/0031-9155/34/6/012.
10. Cheraghian M, Pourfallah T, Sabouri-Dodaran A A, Gholami M. Calculation of photoneutron contamination of varian linac in icru soft-tissue phantom using MCNPX code. J Med Phys. 2021; 46(2): 116. doi: 10.4103/jmp.JMP_40_21.
11. Bezak E, Takam R, Marcu LG. Peripheral photon and neutron doses from prostate cancer external beam irradiation. Radiat Prot Dosim. 2015; 167(4): 591-601. doi: 10.1093/rpd/ncu362.
12. Bezak E, Takam R, Yeoh E, Marcu L G. The risk of second primary cancers due to peripheral photon and neutron doses received during prostate cancer external beam radiation therapy. Phys Med. 2017; 42: 253-258. doi: 10.1016/j.ejmp.2017.02.018.
13. Sohrabi M, Hakimi A. Novel air-to-tissue conversion factors for fast, epithermal and thermal photoneutrons in a Siemens ONCOR dual energy 18 MV X-ray medical linear accelerator. Radiat Meas. 2019; 126: 106138. doi: 10.1016/j.radmeas.2019.106138.
14. Bagheri H, Rabie Mahdavi S, Shekarchi B, Manouchehri F, Farhood B. Measurement of the contralateral breast photon and thermal neutron doses in breast cancer radiotherapy: A comparison between physical and dynamic wedges. Radiat Prot Dosim. 2017; 178(1): 73-81. doi: 10.1093/rpd/ncx076.

15. Bagheri H, Abedi Firouzjah R, Farhood B. Measurement of the photon and thermal neutron doses of contralateral breast surface in breast cancer radiotherapy. J Radiother Pract. 2019: 1-7. doi: 10.1017/S1460396919000578.
16. Barquero R, Mendez R, Vega-Carrillo H R, Iñiguez M P, Edwards T M. Neutron spectra and dosimetric features around an 18 MV Linac accelerator. Health Phys. 2005; 88(1). doi: 10.1097/01. HP.0000142500.32040.ac.
17. Alem-Bezoubiri A, Bezoubiri F, Badreddine A, Mazrou H, Lounis-Mokrani Z. Monte Carlo estimation of photoneutrons spectra and dose equivalent around an 18 MV medical linear accelerator. Radiat Phys and Chem. 2014; 97: 381-392. doi: 10.1016/j.radphyschem.2013.07.013.
18. Martínez-Ovalle SA, Barquero R, Gómez-Ros JM, Lallena AM. Neutron dose equivalent and neutron spectra in tissue for clinical linacs operating at 15, 18 and 20 MV. Radiat Prot Dosim. 2011; 147(4): 498-511. doi: 10.1093/rpd/ncq501.
19. Kry SF, Howell RM, Salehpour M, Followill DS. Neutron spectra and dose equivalents calculated in tissue for high-energy radiation therapy. Med Phys. 2009; 36(4): 1244-1250. doi: 10.1118/1.3089810.
20. Kry SF, Titt U, Followill D, Pönisch F, Vassiliev ON, White RA. A Monte Carlo model for out-of-field dose calculation from high-energy photon therapy. Med Phys. 2007; 34(9): 3489-3499. doi: 10.1118/1.2756940.
21. Kry S F, Titt U, Pönisch F, Followill D, Vassiliev ON, Allen White R. A Monte Carlo model for calculating out-of-field dose from a Varian beam. Med Phys. 2006; 33(11): 4405-4413. doi: 10.1118/1.2360013.
22. Mohammadi N, Miri-Hakimabad H, Rafat-Motavalli L, Akbari F, Abdollahi S. Patient-specific voxel phantom dosimetry during the prostate treatment with high-energy linac. J Radioanal Nucl Chem. 2015; 304(2): 785-792. doi: 10.1007/s10967-014-3872-9.
23. Abou-Taleb WM, Hassan MH, El_Mallah EA, Kotb SM. MCNP5 evaluation of photoneutron production from the Alexandria University 15 MV Elekta Precise medical LINAC. Appl Radiat Isot. 2018; 135: 184-191. doi: 10.1016/j.apradiso.2018.01.036.
24. Toossi MT, Behmadi M, Ghorbani M, Gholamhosseinian H. A Monte Carlo study on electron and neutron contamination caused by the presence of hip prosthesis in photon mode of a 15 MV Siemens PRIMUS linac. J Appl Clin Med Phys. 2013; 14(5): 52-67. doi: 10.1120/jacmp.v14i5.4253.
25. Ghassoun J, Senhou N. The evaluation of neutron and gamma ray dose equivalent distributions in patients and the effectiveness of shield materials for high energy photons radiotherapy facilities. Appl Radiat Isot. 2012; 70(4): 620-624. doi: 10.1016/j.apradiso.2011.12.041.
26. Rezaian A, Nedaie HA, Banaee N. Measurement of neutron dose in the compensator IMRT treatment. Appl Radiat Isot. 2017; 128: 136-141. doi: 10.1016/j.apradiso.2017.06.013.
27. Ghorbani M, Azizi M, Azadegan B, Mowlavi AA, Rahvar ZA, Wagner W. Dosimetric evaluation of neutron contamination caused by dental restorations during photon radiotherapy with a 15 MV Siemens Primus linear accelerator. Radiat Phys Chem. 2020; 174: 108961. doi: 10.1016/j.radphyschem.2020.108961.
28. Chegeni N, Karimi AH, Jabbari I, Arvandi S. Photoneutron dose estimation in GRID therapy using an anthropomorphic phantom: A monte carlo study. J med signals sens. 2018; 8(3): 175. doi: 10.4103/jmss.JMSS_13_18.
29. Gao Q, Zha H, Chen H, Shi J. Design and optimization of the target in electron linear accelerator. Proceedings

of IPAC2013, Shanghai, China, 2013; 1(745.52): 0.05.

30. Berger MJ, Seltzer SM. Bremsstrahlung and photoneutrons from thick tungsten and tantalum targets. Phys Rev C. 1970; 2(2): 621. doi: 10.1103/PhysRevC.2.621.
31. Rojas-Arias N, Sajo-Bohus L, Tolosa-Cetina JO, Sandoval-Garzon MA, Martinez-Ovalle SA. New target with low photoneutron yield for LINAC radiotherapy applications. Appl Radiat Isot. 2020; 162: 109142. doi: 10.1016/j.apradiso.2020.109142.
32. Podgorsak E, Rawlinson J, Glavinovic M, Johns H. Design of X-ray targets for high energy linear accelerators in radiotherapy. Am J Roentgenol. 1974; 121(4): 873-882.
33. Pena J, Franco L, Gómez F, Iglesias A, Pardo J, Pombar M. Monte Carlo study of Siemens PRIMUS photoneutron production. Phys Med Biol. 2005; 50(24): 5921. doi: 10.1088/0031-9155/50/24/011.
34. Dowlatabadi H, Mowlavi AA, Ghorbani M, Mohammadi S, Knaup C. Study of photoneutron production for the 18 mv photon beam of the siemens medical linac by monte carlo simulation. J Biomed Phys & Eng. 2020; 10(6): 679. doi: 10.31661/JBPE.V0I0.939.
35. Farhood B, Ghorbani M, Goushbolagh NA, Najafi M, Geraily G. Different methods of measuring neutron dose/fluence generated during radiation therapy with megavoltage beams. Health phys. 2020;118(1):65-74. doi: 10.1097/HP.0000000000001130.